Bone Reports 14 (2021) 100757

Contents lists available at ScienceDirect

Bone Reports

journal homepage: www.elsevier.com/locate/bonr

Low magnetic field promotes recombinant human BMP-2-induced bone formation and influences orientation of trabeculae and bone marrow-derived stromal cells

Rintaro Okada [a], Kai Yamato [b], Minoru Kawakami [b], Joe Kodama [a], Junichi Kushioka [a], Daisuke Tateiwa [a], Yuichiro Ukon [a], Bal Zeynep [a], Takuya Ishimoto [c], Takayoshi Nakano [c], Hideki Yoshikawa [d], Takashi Kaito [a,*]

[a] Department of Orthopedic Surgery, Osaka University Graduate School of Medicine, Suita, Osaka, Japan
[b] Department of Research Institute, PIP Corporation, Ibaraki, Osaka, Japan
[c] Division of Materials and Manufacturing Science, Osaka University Graduate School of Engineering, Suita, Osaka, Japan
[d] Department of Orthopedic Surgery, Toyonaka Municipal Hospital, Toyonaka, Osaka, Japan

ARTICLE INFO

Keywords:
Magnetic field
Bone marrow-derived stromal cells
Osteoblastic differentiation
Orientation intensity
Mechanical strength

ABSTRACT

Effects of high magnetic fields [MFs, ≥ 1 T (T)] on osteoblastic differentiation and the orientation of cells or matrix proteins have been reported. However, the effect of low MFs (< 1 T) on the orientation of bone formation is not well known. This study was performed to verify the effects of low MFs on osteoblastic differentiation, bone formation, and orientation of both cells and newly formed bone. An apparatus was prepared with two magnets (190 mT) aligned in parallel to generate a parallel MF. *In vitro*, bone marrow-derived stromal cells of rats were used to assess the effects of low MFs on cell orientation, osteoblastic differentiation, and mineralization. A bone morphogenetic protein (BMP)-2-induced ectopic bone model was used to elucidate the effect of low MFs on microstructural indices, trabecula orientation, and the apatite *c*-axis orientation of newly formed bone. Low MFs resulted in an increased ratio of cells oriented perpendicular to the direction of the MF and promoted osteoblastic differentiation *in vitro*. Moreover, *in vivo* analysis demonstrated that low MFs promoted bone formation and changed the orientation of trabeculae and apatite crystal in a direction perpendicular to the MF. These changes led to an increase in the mechanical strength of rhBMP-2-induced bone. These results suggest that the application of low MFs has potential to facilitate the regeneration of bone with sufficient mechanical strength by controlling the orientation of newly formed bone.

1. Introduction

Pulsed electromagnetic field (PEMF) technology is widely used to promote fracture healing (Murray and Pethica, 2016). However, PEMF devices require electric power and are associated with limited time for patients to receive treatment and activity. The static magnetic field (MF) generated by permanent magnets has several therapeutic advantages, such as no requirement of a power device and creation of the MF in the intended direction, making MF stimulation more suitable for long-term local healing.

Static MFs, even low MFs [< 1 T (T)], have been reported to accelerate osseous fusion and to promote osteoblastic differentiation at a cellular level (Aydin and Bezer, 2011; Yuge et al., 2003; Bruce et al., 1987; Yamamoto et al., 2003). In addition, static high MFs (≥ 1 T) are

Abbreviations: PEMF, pulsed electromagnetic field; MF, magnetic field; BMDCs, bone marrow derived stromal cells; rhBMP, recombinant human bone morphogenetic protein; GFP, green fluorescent protein; PBS, phosphate-buffered saline; ALP, alkaline phosphatase; RT-PCR, reverse transcription polymerase chain reaction; COL1a1, collagen type1 a1; OCN, osteocalcin; OSX, osterix; OPN, osteopontin; RUNX2, runt-related transcription factor 2; micro-CT, micro-computed tomography; BV, bone volume; ROI, region of interest; BMD, bone mineral density; FFT, fast Fourier transform; μXRD, microbeam X-ray diffractometer.

* Corresponding author at: Department of Orthopaedic Surgery, Osaka University Graduate School of Medicine, 2-2 Yamadaoka, Suita, Osaka 565-0871, Japan.
E-mail addresses: rintaro-okada@umin.ac.jp (R. Okada), k-yamato@pipjapan.co.jp (K. Yamato), m-kawakami@pipjapan.co.jp (M. Kawakami), ishimoto@mat.eng.osaka-u.ac.jp (T. Ishimoto), nakano@mat.eng.osaka-u.ac.jp (T. Nakano), yhideki@chp.toyonaka.osaka.jp (H. Yoshikawa), takashikaito@ort.med.osaka-u.ac.jp (T. Kaito).

https://doi.org/10.1016/j.bonr.2021.100757
Received 9 July 2020; Received in revised form 16 January 2021; Accepted 17 February 2021
Available online 22 February 2021

reported to regulate the orientation of cells and bone matrix proteins (Kotani et al., 2000; Kotani et al., 2002; Shinohara et al., 2006). These results suggest that static MFs have the potential to promote the healing of bone with mechanical strength by controlling the orientation of bone matrix. However, the effect of low MFs on the orientation of bone matrix has not been demonstrated. The size of high MF generators and health issues (such as nausea and vertigo) related to high MFs prevent their clinical application (Schenck, 2000). However, if the effect of static MFs on orientation can be demonstrated even with low MFs, their application for bone fracture treatment is expected to promote early and functional bone regeneration. The aim of this study was to verify the effects of low MFs (190 mT) on osteoblastic differentiation and cell orientation in rat bone marrow-derived stromal cells (BMDCs) *in vitro* and to elucidate the effects on bone formation and orientation of the bone matrix based on recombinant human bone morphogenetic protein (rhBMP)-2-induced ectopic bone formation *in vivo*. Our results provide a basis for development of low MF generators that are safer and more practical for treatment of bone fractures.

2. Materials and methods

2.1. In vitro experiments

2.1.1. Preparation of BMDCs and cell culture

Rat BMDCs were obtained from the femurs of green fluorescent protein (GFP) transgenic rats (SD-Tg (CAG-eGFP), 3-week-old, male; Japan SLC Co. Ltd., Shizuoka, Japan). BMDCs were collected as described previously (Gao et al., 2001). Dissected femurs were cut at both ends and flushed with 2 mL of α-MEM (Nacalai Tesque, Inc., Kyoto, Japan) using a needle and a syringe to obtain bone marrow. The extracted bone marrow from the two femurs was seeded into 150-mm culture dishes with 16 mL of culture medium composed of DMEM (Nacalai Tesque, Inc.) containing 10% fetal bovine serum (Gibco, Grand Island, NY, USA) and 1% antibiotics (penicillin, streptomycin, and fungizone; Sigma-Aldrich Corp., St. Louis, MO, USA). The dishes were incubated in a humidified atmosphere with 5% CO_2 at 37 °C. After 3 days of culture, the dishes were washed thoroughly with phosphate-buffered saline (PBS) to remove non-adherent cells. The medium was changed every 3 days. When the cells reached 80% confluence, they were detached using 0.25% trypsin and 1 mM EDTA (Gibco, Grand Island) and passaged. BMDCs at the second passage were used for all experiments in this study. Osteogenic differentiation medium was prepared by adding 10 nM dexamethasone, 10 mM β-glycerophosphate, and 50 μM ascorbic acid to the culture medium.

2.1.2. Magnetic apparatus for in vitro experiments

For *in vitro* experiments, two magnetic rectangular plates (MF group; 100 mm length × 10 mm width × 2 mm height; made of neodymium, 190 mT, Pip Co., Ltd., Osaka, Japan) were aligned 10 mm apart with both sides of an 8-well strip plate to generate a parallel MF (Fig. 1A). For the apparatus used in the control group, non-magnetic rectangular plates with the same dimensions were used.

2.1.3. Cell orientation assay

The orientation of the cells was measured by modification of a previously described method (Matsugaki et al., 2015). The analysis was performed at day 2 after BMDCs were seeded into 8-well plates (2000 cells/well, $n = 10$, Corning Inc.) containing culture medium. Ten wells were analyzed with at least 150 cells/well. Briefly, photographs of the cells at the center of each well were taken using a fluorescence microscope (BZ-X700, Keyence, Osaka, Japan). The cells in the images were extracted with an image analysis software (BZ-X Analyzer, Keyence). The extracted cell images were converted to binarization using the ImageJ software (National Institutes of Health, Bethesda, Maryland). Cell orientation was analyzed quantitatively using the Cell Profiler software (Broad Institute, Cambridge, MA).

2.1.4. Alkaline phosphatase (ALP) activity

ALP activity was determined at days 5, 8, and 12 after BMDCs were seeded using a LabAssay™ ALP assay kit (Wako Pure Chemical Co., Osaka, Japan). The BMDCs were seeded into an 8-well plate (5000 cells/well, $n = 8$) containing osteogenic differentiation medium. The BMDCs were washed in PBS three times and lysed with 0.1% Triton X-100 solution (Nacalai Tesque, Inc.). Total protein concentrations were determined using the Bradford protein assay method and ALP activity was normalized to the total protein concentrations.

2.1.5. Alizarin-red staining

Mineralization was evaluated by quantifying the formation of mineralized nodules using an Alizarin-red staining assay. Alizarin-red

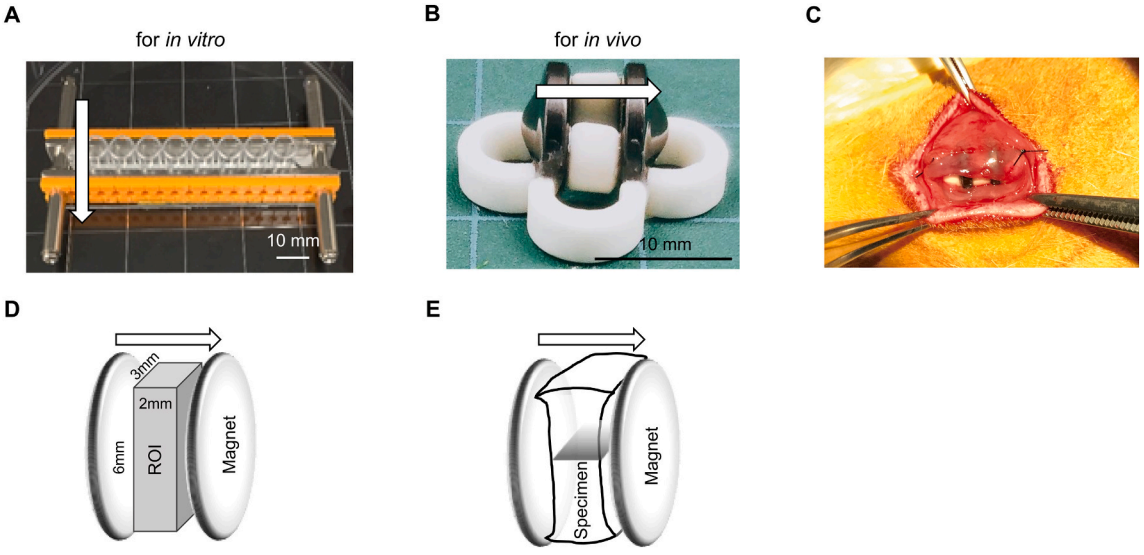

Fig. 1. Magnetic apparatuses used in this study. (A) Photograph of magnetic apparatus used *in vitro*. (B) Photograph of magnetic apparatus used *in vivo*. (C) Photograph of the apparatus installed under the fascia during surgery. (D) The region of interest (ROI) was set for the analysis of micro structure at post-operative 3 weeks. (E) Trabecula orientation was analyzed using the center level of the micro-computed tomography image, which was perpendicular to the longitudinal direction of the specimen (gray parallelogram area). White arrows indicate the direction of the magnetic field.

staining was performed at day 10 after BMDCs were seeded into 8-well plates (5000 cells/well, n = 8) containing osteogenic differentiation medium. Cells were fixed with 70% ethanol for 30 min, washed in PBS, and stained with 40 mM Alizarin-red solution at pH 4.2 (Muto Pure Chemicals Co. Ltd., Tokyo, Japan) for 10 min. Each well was rinsed three times with pure water and photographed after drying. Mineralized nodules were dissolved in 5% formic acid. For semi-quantitative evaluation, 100 μL of each solution was transferred to 96-well plates. Subsequently, absorbance was measured at 450 nm using a microplate reader (Multiskan Go, Thermo Fisher Scientific K.K., Tokyo, Japan).

2.1.6. RNA isolation and reverse transcription polymerase chain reaction (RT-PCR) analysis

The expression of the following six genes involved in osteogenesis in BMDCs was analyzed using real-time RT-PCR: *ALP*, collagen type1 a1 (*COL1a1*), osteocalcin (*OCN*), osterix (*OSX*), osteopontin (OPN), and runt-related transcription factor 2 (*RUNX2*). The primer sequences of osteogenic genes are listed in Table 1. RNA was extracted from BMDCs seeded in 8-well plates (5000 cells/well, $n = 4$) containing osteogenic differentiation medium and cultured for 2 and 5 days. Total RNA was extracted using a RNeasy Mini Kit (Qiagen, Valencia, CA, USA), and RNA concentrations were measured with a Nanodrop 1000 instrument (NanoDrop Technologies, Wilmington, DE). Total RNA (200 ng) was reverse-transcribed using a cDNA synthesis kit (ReverTra Ace qPCR RT Master Mix; Toyobo Co., Ltd., Osaka, Japan). The cDNA was stored at −30 °C. RT-PCR was performed using the SYBR Green PCR Master Mix (Applied Biosystems, Foster City, CA). Each sample was analyzed in duplicate, and the relative quantity of mRNA was calculated using the $2^{-\Delta\Delta Ct}$ relative quantification method. The mRNA expression of each target gene was normalized to that of the housekeeping gene, glyceraldehyde-3-phosphate dehydrogenase (*GAPDH*).

2.1.7. Western blot analysis

Proteins were extracted from BMDCs seeded in 8-well plates (5000 cells/well) containing osteogenic differentiation medium and cultured for 5 and 7 days. Cells were lysed in RIPA buffer (Thermo Fisher Scientific) supplemented with 1% phosphatase inhibitor cocktail (Nacalai Tesque, Inc.). The lysates were sonicated, centrifuged at 12,000 rpm for 5 min at 4 °C, and the supernatants were used for electrophoresis after determining the protein concentration using BCA assay kit (Thermo Fisher Scientific). The separated proteins were transferred onto a polyvinylidene fluoride membrane. After blocking with phospho-blocker (Cell Biolabs Inc., San Diego, CA) for 1 h, the membrane was probed overnight at 4 °C with a primary antibody (RUNX2 antibody, 1:1000; #8486, Cell Signaling Technology, Danvers, MA, USA) and subsequently with anti-rabbit IgG HRP-linked antibody (Cell Signaling Technology) for 1 h at room temperature. An ECL plus Western Blotting Detection System kit (GE Healthcare, UK) was used to detect the signals. β-actin was used as the loading control.

2.1.8. Effects of different MF intensities on BMDCs

To investigate the effects of different MF intensities, we created an extreme-low MF environment (ex-low MF group; 60 mT) for *in vitro* cell culture by almost doubling the distance between two magnetic plates (22 mm) compared to the distance between the two magnetic plates in the low MF apparatus (10 mm) (Supplementary Fig. S1). Cell orientation and ALP activity were compared among the control, the ex-low MF, and the MF groups.

Table 1
Primers used in this study.

Gene	Forward (5′-3′)	Reverse (5′-3′)
ALP	TGGAAGGAGGCAGGATTGAC	CCGATGGCCTCATCCATCTC
COL1A1	TCCTGACGCATGGCCAAGAA	CATAGCACGCCATCGCACAC
OCN	CCGGCCTGAGAGAGGAGAA	CTCAAGAGGTCTGGCACGAA
OSX	CGGCCTGAGAGAGGAGAAGA	CAAGAGGTCTGGCACGAAGA
OPN	CCAGCCAAGGACCAACTACAA	GTAATGCGCCTTCTCCTCTGA
RUNX2	ACCACAAGTGCGGTGCAA	GTTGGTCTCGGTGGCTGGTA
GAPDH	GTGCCAGCCTCGTCTCATAG	CGTTGATGGCAACAATGTCC

2.2. In vivo experiments

2.2.1. Animals

All animal experiments in this study were performed according to the animal welfare guidelines and were approved by the animal ethics committee of our facility. Twenty-eight 8-week-old male Sprague-Dawley rats (Charles River Labs. Japan Inc., Kanagawa, Japan) were used.

2.2.2. Preparation of collagen sponge containing recombinant human bone morphogenetic protein (rhBMP)-2

rhBMP-2 (10 μg; Osteopharma Inc., Osaka, Japan) was dissolved in 120 μL PBS, soaked into an absorbable collagen sponge (punched out in a cylindrical shape, 5 mm diameter × 10 mm length; Integra LifeSciences, Plainsboro, NJ, USA), and freeze-dried (Free Zone 2.5, Labconco, MO, USA).

2.2.3. Magnetic apparatus for in vivo experiments

For *in vivo* experiments, two circular plates (MF group, 8 mm diameter × 2 mm height; made of ferrite, 190 mT, Pip Co., Ltd., Osaka, Japan) were aligned in parallel to generate a parallel MF (Fig. 1B). For the apparatus used in the control group, non-magnetic rectangular plates with the same dimensions were used.

2.2.4. Surgical technique

The rats were anesthetized using a combination of 0.15 mg/kg medetomidine (Nippon Zenyaku Kogyo Co., Ltd., Fukushima, Japan), 2.0 mg/kg midazolam (Astellas Pharma, Inc., Tokyo, Japan), and 2.5 mg/kg butorphanol (Meiji Seika Pharma Co., Ltd., Tokyo, Japan). A 3-cm midline incision was made at the back of rats, and a pocket was made by dividing the fascia and muscle using an elevatorium. The apparatus was implanted into the pocket after the rhBMP-2 soaked collagen sponge was placed between the magnets. Both ends of the apparatus were sutured with fascia to prevent migration (Fig. 1C). All rats were euthanized with carbon dioxide at post-operative weeks 3 or 6 ($n = 16$ and 12, respectively), and the magnetic apparatus including ectopic bone was harvested and fixed with 70% ethanol.

2.2.5. Micro-computed tomography

The newly formed bone extracted from the apparatus was scanned using high-resolution micro-computed tomography (micro-CT, SkyScan1272; Bruker, Kontich, Belgium) at 3- and 6-weeks post-operation. Micro-CT was performed under parameters of 70 kV and 140 μA at a resolution of 10 μm/voxel. Visualization and data reconstruction were performed using two software (NRecon and CTan; Bruker).

2.2.6. Microstructural analysis of newly formed bone

The microstructure of newly formed bone in the apparatus was assessed based on micro-CT images. Microstructural indices included bone volume (BV), bone surface, trabecular thickness, trabecular separation, and trabecular number. Microstructural analysis was performed to evaluate the effect of low MFs on bone formation at 3 weeks post-operation. The region of interest (ROI) was set as a region where the parallel MF existed definitely in the specimen. The ROI was determined to be in the middle of the space between magnets, 6 mm in length × 3 mm in width × 2 mm in height (Fig. 1D). Bone mineral density (BMD) of total newly formed bone was analyzed at 6 weeks post-operation.

2.2.7. Trabecula orientation analysis of newly formed bone

At 6 weeks post-operation, the trabecula orientation of newly formed bone at the center of the apparatus was analyzed using the micro-CT image, which was perpendicular to open windows of the apparatus.

(Fig. 1E). The micro-CT image was binarized with ImageJ and converted by fast Fourier transform (FFT) using a fiber orientation analysis software (FiberOri8single03; Tsukuba University, Ibaraki, Japan) (Enomae, 2019; Enomae et al., 2006). An approximate ellipse was drawn from the plot of amplitudes of the FFT image (Fig. 2A). The orientation angle was shown as the angle between the minor axis of the approximate ellipse and the *x*-axis (x > 0, angle range was from −90 to 90 degrees). The orientation intensity (≥ 1) was calculated from the length ratio of the major/minor axis of the approximate ellipse.

2.2.8. Analysis of apatite c-axis orientation

The degree of the apatite *c*-axis orientation was analyzed with a microbeam X-ray diffractometer (μXRD) system (R-Axis BQ, Rigaku, Tokyo, Japan) equipped with a transmission-type optical system and an imaging plate (storage phosphors; Fuji Film, Tokyo, Japan) placed behind the specimen. The crystallographic apatite orientation is an important characteristic at the nanometer-scale to determine the mechanical properties of bone tissues including regenerated bones (Ishimoto et al., 2013). The apatite orientation mirrors collagen fiber orientation because crystallization on the collagen template occurs in an epitaxial manner through an *in vivo* self-assembly process; therefore, the analysis of apatite *c*-axis orientation indirectly refers to the orientation of collagen fibers (Landis, 1995). The apatite (and collagen) orientation is independent of the trabecular alignment and represents the anisotropy of the atomic arrangement within trabeculae (Ishimoto et al., 2018). Mo-Kα radiation was generated at a tube voltage of 50 kV and a tube current of 90 mA. The distance between the detector and the X-ray focus of the specimen was 127.4 mm. The pixel size of the imaging plate was 100 × 100 μm. The incident beam was focused on a beam spot of 800 μm diameter by a double-pinhole metal collimator. The transmission method with Mo-Kα radiation enables the analysis of the two-dimensional distribution of diffraction information perpendicular to the incident beam (Ishimoto et al., 2018). The direction of the measured apatite orientation in the specimen was defined as shown in Fig. 2B (MF direction and major/minor axis direction). The major axis direction was defined as the direction perpendicular to the MF and the longitudinal direction of the specimen. The minor axis direction was defined as a direction perpendicular to the MF and lateral direction of the specimen. The incident X-ray was radiated in two directions on the specimen (MF direction and minor axis direction) to detect diffraction information (along the major axis and minor axis direction, MF direction, and major direction, respectively) to analyze the effect of the MF on apatite orientation. The diffraction data were collected for 60 s. From the obtained diffraction intensity pattern (Debye ring), the intensity of the diffracted beam from the aforementioned directions was converted as a function of 2θ to describe the X-ray diffraction profile. The ratio of the integrated intensity of (002) to that of (310) was calculated to quantitatively analyze the degree of apatite *c*-axis orientation (Nakano et al., 2002). The measurement was repeated three times with an interval of 1 mm along the major axis of the specimen.

2.2.9. Biomechanical testing of newly formed bone

A compression test was performed to analyze the mechanical strength (Instron 5565, Instron, Norwood, MA, USA). The compressive direction was set in the minor axis direction (Fig. 3) to investigate the benefit of MF exposure. Load and displacement data were acquired every 10 ms and converted to a stress–strain curve using dimensions of the specimen, as determined from the micro-CT data. From the load-displacement curve, the ultimate load at failure (N; maximum force that the bone could bear) and stiffness (S, N/mm; slope of the load-displacement curve at the linear part) were measured. Young's modulus (MPa; slope of the stress–strain curve at the linear part) and ultimate stress (MPa; maximum stress that the bone could bear) were evaluated.

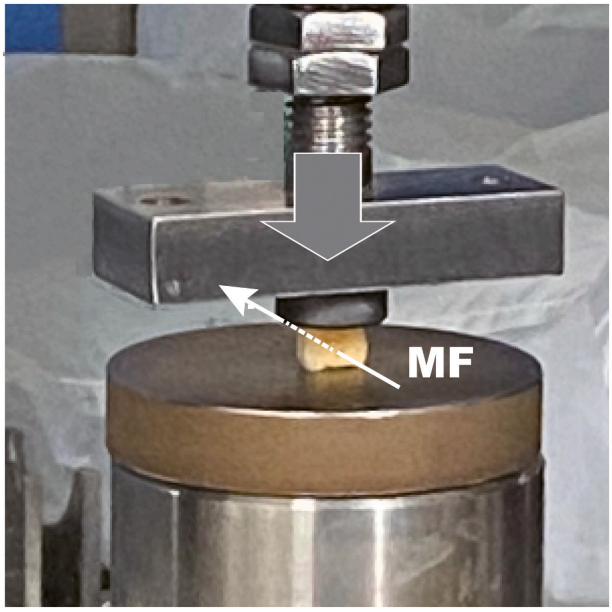

Fig. 3. Compression test photograph. The compression test was performed in the minor axis (perpendicular direction to the magnetic field [MF] and lateral direction of the specimen). The solid arrow with a dark area indicates the compressive direction.

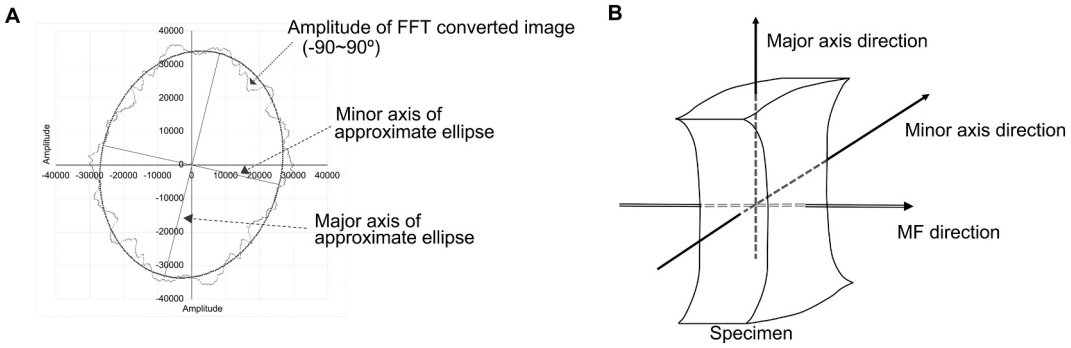

Fig. 2. (A) An example of the result of trabecula orientation analysis. Amplitudes of fast Fourier transform (FFT) images from −90 to 90 degree were plotted. Amplitudes from 90 to −90 degrees were point-symmetric to the origin. An approximate ellipse of the amplitudes was drawn. The orientation angle (from −90 to 90 degrees) is shown as the angle between the minor axis and the *x*-axis. The orientation intensity (≥ 1) was calculated from the ratio of the major axis length to the minor axis length. (B) Triaxial directions were defined in the specimen as shown. The longitudinal direction to the specimen and perpendicular direction to the magnetic field (MF) were defined as the major axis. The lateral direction to the specimen and perpendicular direction to the MF were defined as the minor axis.

2.3. Statistical analysis

All statistical analyses were performed with EZR (Saitama Medical Center, Jichi Medical University, Saitama, Japan). The EZR is a graphical user interface for R (The R Foundation for Statistical Computing, Vienna, Austria, version 3.5.0) (Kanda, 2013). The data were analyzed using the Kolmogorov-Smirnov test to compare the cell orientation distribution, and Student's *t*-test was used to compare other results. An F-test was used to compare the standard deviation of the trabecula orientation angle. ALP activity among multiple groups was analyzed with one-way analysis of variance (ANOVA) followed by Dunnett's test. In all analyses, the statistical significance threshold was set at $p < 0.05$.

3. Results

3.1. Cell orientation analysis

A significant difference in the distribution of the cell orientation angle was demonstrated between the groups ($p = 0.005$, Fig. 4B). The ratio of cells oriented perpendicular to the direction of the MF was increased. There was no significant difference in the average orientation angle between the control group and the MF group.

3.2. Osteoblastic differentiation and mineralization of BMDCs

ALP activity in the MF group continued to increase until day 12 after inducing differentiation and was significantly higher than that in the control group at that time (control: 2.76 ± 0.32, MF: 4.63 ± 0.62 units/μg protein, p = 0.005; Fig. 5A). Mineralization, which was determined by dissolving nodules, was significantly increased with MF application (control: 0.74 ± 0.10, MF: 0.87 ± 0.11 AU, $p = 0.03$; Fig. 5B). The RT-PCR results at day 2 and 5 are shown in Fig. 5C. Low MF treatment increased the relative mRNA expression of *RUNX2* at day 2 (control: 1.21 ± 1.90, MF: 2.07 ± 0.36, $p = 0.02$) and *ALP* at day 5 (control: 1.08 ± 0.08, MF: 1.81 ± 0.21, $p = 0.03$) compared with that in the control group. The RUNX2 expression was upregulated in the MF group on day 5 (Fig. 5D).

3.3. Effects of extremely low MF intensity on BMDCs

Although the cell orientations between the control and the low MF group were significantly different, no significant difference was found between the control and the ex-low MF groups (control *vs.* ex-low MF: $p = 0.83$, control *vs.* low MF: p = 0.02, Supplementary Fig. S2A). ALP activity in the ex-low MF group showed an increasing trend compared to the control group, but the difference was not statistically significant (control *vs.* ex-low MF: $p = 0.37$, control *vs.* low MF: p = 0.02, Supplementary Fig. S2B).

3.4. Micro structural analysis of newly formed bone

Representative micro-CT three-dimensional images are shown (Fig. 6A). In the MF group, new bone formation reaching to the center of the apparatus was observed. The results of microstructural analysis *via* micro-CT scanning are shown in Fig. 6B. At 3 weeks post-operation, the BV in the MF group was significantly increased compared with that in the control group (control: 4.14 ± 1.85, MF: 6.49 ± 1.88 mm^3, p = 0.03). At 6 weeks post-operation, BMD in the MF group was significantly larger than that in the control group (control: 0.25 ± 0.05, MF: 0.36 ± 0.06 g/cm^3, $p = 0.004$; Fig. 6C).

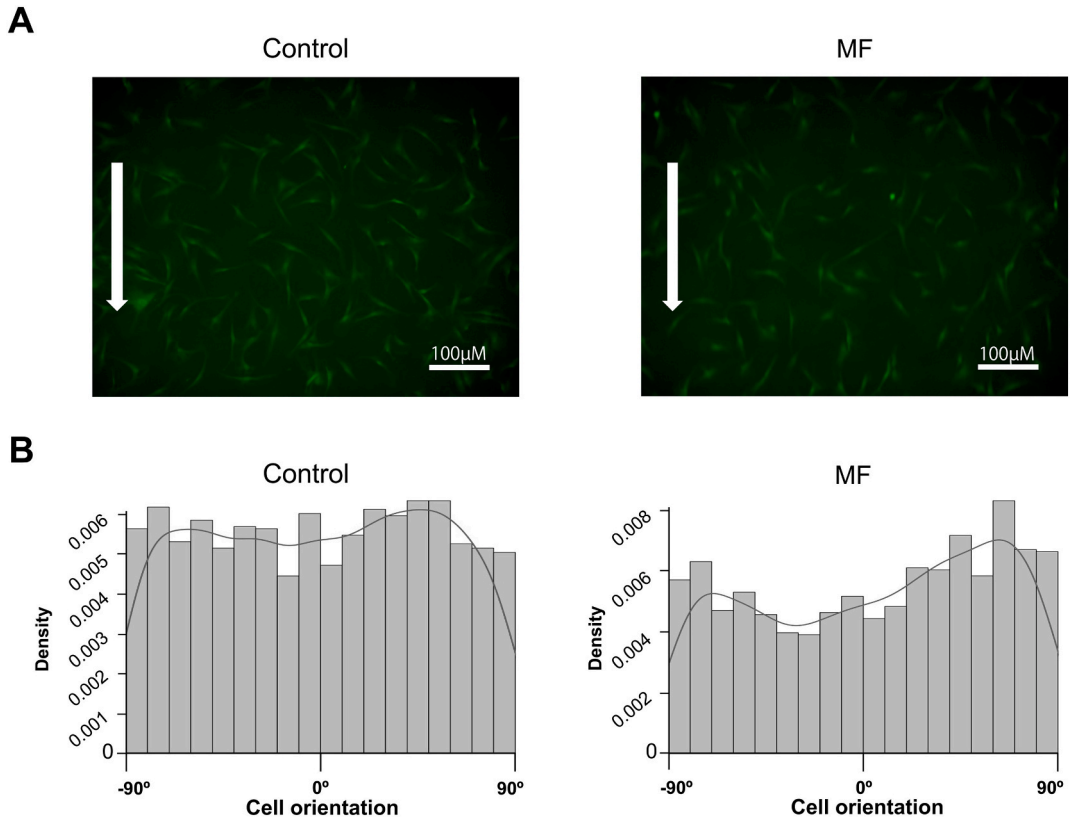

Fig. 4. Cell orientation after magnetic field (MF) exposure. (A) Bone marrow-derived cells cultured after 48 h of exposure to a 190 mT MF. White arrows indicate the direction of the MF. (B) Distribution of the cell orientation angle. The ratio of cells distributed near −90 or 90 degrees, which is the MF direction, was increased with the application of a low MF. The distributions between the two groups were significantly different (p = 0.005).

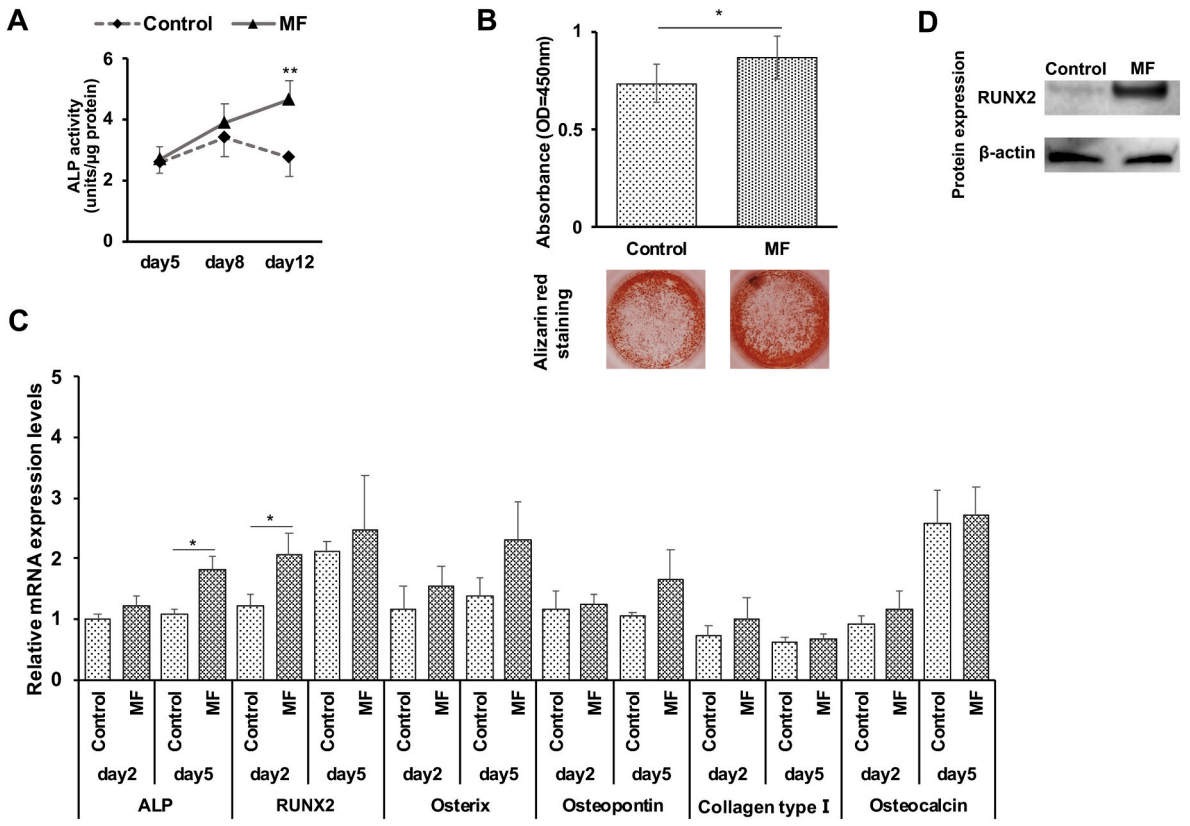

Fig. 5. Effects of low magnetic fields (MFs) on osteoblastic differentiation. (A) Alkaline phosphatase activity in the MF group continued to increase until day 12 after cells were seeded. Statistical significance was indicated as follows: ** $p < 0.01$. (B) Absorbance of mineralized nodules and photos of alizarin-red staining. Mineralization was promoted by the application of a low MF. Statistical significance is indicated as follows: * $p < 0.05$. (C) Relative gene expression levels of bone-related markers. The expression of *RUNX2* and *ALP* in the MF group was higher than that in the control group. Quantitative reverse transcription-polymerase chain reaction data were normalized to glyceraldehyde-3-phosphate dehydrogenase levels. Statistical significance is indicated as follows: * $p < 0.05$. (D) On day 5, the expression of RUNX2 was higher in MF group than in the control group.

3.5. Orientation analysis of trabecular bone

The results of trabecular bone orientation analysis are shown in Table 2. The degree of trabecular bone orientation was $8.65 \pm 29.22°$ in the control group and -6.09 ± 9.33 in the MF group. Mean values of cell orientation angle were not significantly different ($p = 0.31$). In contrast, variation in each group showed a significant difference ($p = 0.026$). Trabecular bone orientation intensity in the MF group was significantly increased relative to that in the control group (control: 1.25 ± 0.10, MF: 1.72 ± 0.23, $p = 0.002$).

3.6. Orientation analysis of apatite c-axis

The results of apatite orientation analysis are shown in Table 3. The intensity of apatite *c*-axis orientation in the MF group was significantly higher than that in the control group along the minor axis direction (perpendicular to the MF) of the specimen (control: 0.68 ± 0.10, MF: 0.96 ± 0.22, $p = 0.029$). The degree of apatite *c*-axis between values along the minor axis direction (perpendicular to the MF) and along the MF direction was significantly different in the MF group (0.96 ± 0.22 and 0.65 ± 0.15, respectively; $p = 0.001$); in contrast, no difference was observed in the control group (0.68 ± 0.10 and 0.60 ± 0.04, respectively; $p = 0.106$).

3.7. Biomechanical testing of the newly formed bone

Both Young's modulus and ultimate stress in the MF group (Young's modulus: 11.47 ± 1.74 MPa, ultimate stress: 4.04 ± 2.14 MPa) were significantly higher than those in the control group (Young's modulus: 4.96 ± 2.70 MPa, ultimate stress: 1.73 ± 1.03 MPa; $p = 0.0006$ and 0.039, respectively; Table 4).

4. Discussion

In this study, we demonstrated that a static low MF could affect the orientation of cells and bone matrix, in addition to osteoblastic differentiation, *in vitro*. Further, the changes in bone matrix orientation led to increased mechanical strength in the direction perpendicular to the MF *in vivo*.

The effects of a static low MF on osteoblastic differentiation have been controversial (Yamamoto et al., 2003; Kim et al., 2017). Regarding the effects of low MFs on osteoblastic differentiation, it has been reported that MF stimulation activates BMP-2 expression, which induces RUNX2, an osteoblast-specific-transcription factor (Yun et al., 2016). Furthermore, low MFs were reported to activate BMP-2 downstream signaling, such as Smad1/5/8, Wnt, MAPK, and NF-κB pathways (Kim et al., 2017; Yun et al., 2016). The *in vitro* results of this study, including the upregulation of RUNX2 and ALP mRNA expression, and increase in ALP activity and RUNX2 expression support the beneficial effects of a static low MF on osteoblastic differentiation. In addition, the static low MF enhanced ectopic bone formation *in vivo*. Our results suggest that the application of low MF may help to provide bone quality improvement by promoting mineralization, because the BMD depends on both the amount of bone mass and bone mineralization. Further studies are needed to verify the effects of low MFs on mineralization.

The effects of static low MFs on cell orientation have so far been demonstrated with several cells (human umbilical-cord-derived mesenchymal stem cells and human glioblastoma cells) (Sadri et al.,

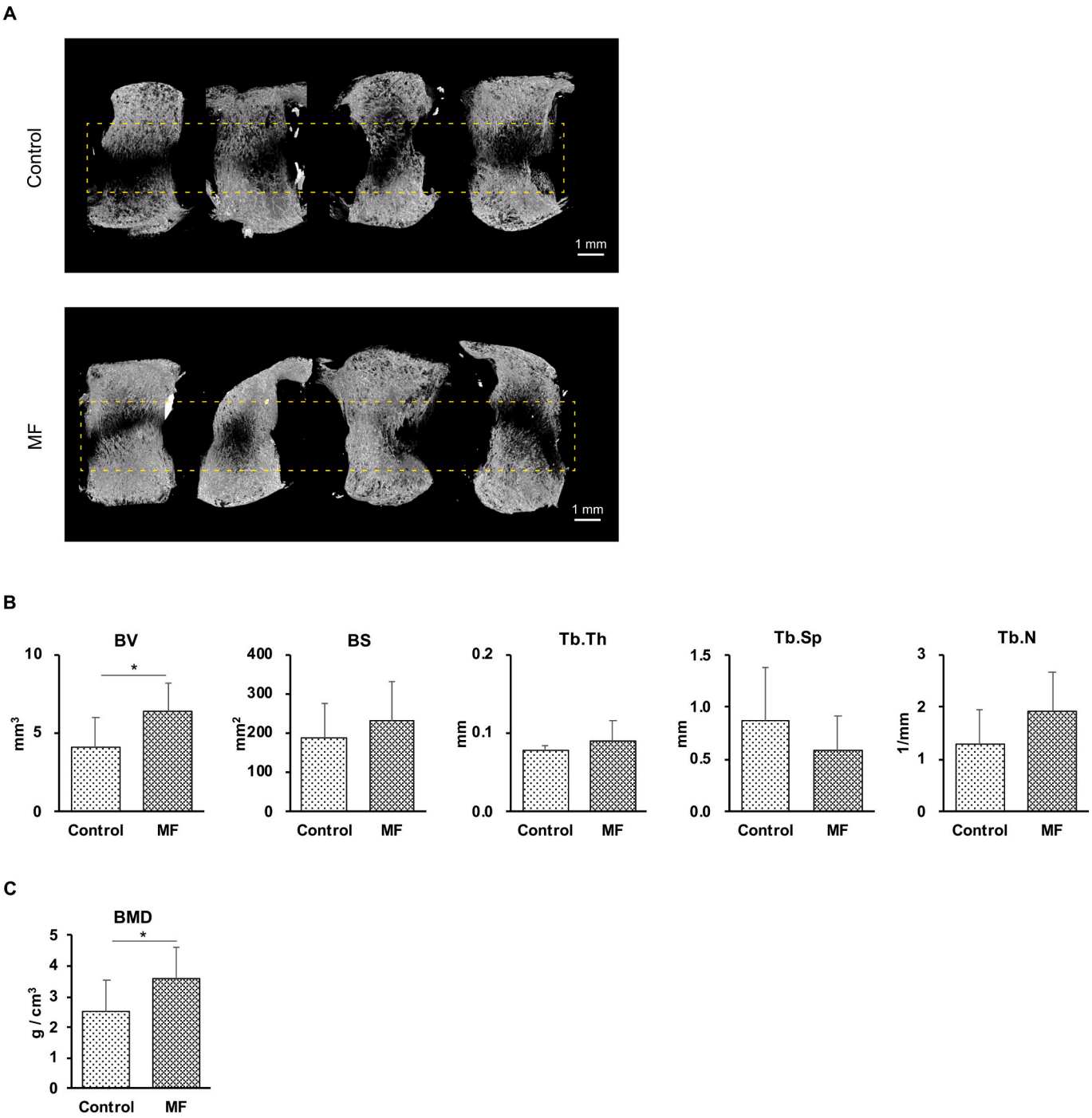

Fig. 6. Bone parameters after magnetic field (MF) application. (A) Three-dimensional images, which were reconstructed from microcomputed tomography data, at post-operative 3 weeks. More advanced bone formation toward the center of the apparatus in the MF group was observed (yellow dashed square area). (B) The results of micro structure analysis of newly formed bone at post-operative 3 weeks in the region of interest. There was a significant difference in bone volume between the groups. Statistical significance is indicated as follows: * $p < 0.05$. (C) The results of BMD at post-operative 6 weeks. Statistical significance is indicated as follows: * $p < 0.05$. BV, bone volume; BS, bone surface; Tb.Th, trabecular thickness; Tb.Sp, trabecular separation; Tb.N, trabecular number; BMD, bone mineral density.

Table 2
Trabecular orientation in recombinant human (rh)BMP-2-induced bone.

	Control	MF	T-test *p*-value	F-test p-value
Orientation angle (°)	8.65 ± 29.22	−6.09 ± 9.33	0.31	0.026
Orientation intensity	1.25 ± 0.10	1.75 ± 0.23	0.025	N/A

Table 3
Apatite *c*-axis orientation in recombinant human (rh)BMP-2-induced bone.

Direction	Control	MF	p-value
Major axis	1.49 ± 0.28	1.62 ± 0.20	0.39
MF	0.60 ± 0.04	0.65 ± 0.15	0.54
Minor axis	0.68 ± 0.10	0.96 ± 0.22	0.029

Table 4
Mechanical strength of recombinant human (rh)BMP-2-induced bone.

	Control	MF	p-value
Ultimate stress (MPa)	1.73 ± 1.03	4.04 ± 2.14	0.039
Young's modulus (MPa)	4.96 ± 2.70	11.47 ± 1.74	0.0006

2017; Teodori et al., 2006). In the present study, we show for the first time that static low MFs could influence the orientation of BMDCs, specifically in a direction parallel to the MF. The mechanism through which the MF influences adherent cell orientation is unknown; however, it has been considered to involve membrane surface components (Umeno and Ueno, 2003). For example, hydrocarbon chains of the phospholipid bilayer, comprising the cell membrane, exhibit the property of diamagnetism (Higashi et al., 1993). When a diamagnetic material is applied to the MF, the rotational magnetic torque, which is caused by anisotropic susceptibility, acts on the hydrocarbon chains. Our results suggest that the main axis direction of rod-shaped cells is aligned parallel to the low MF direction, that is, the hydrocarbon chains were aligned perpendicular to the low MF direction to counteract the rotation torque of cells.

As for the effects of MF intensity, our results suggested that 190 mT low MF is an approximate lower limit that can influence on both cell orientation and osteoblastic differentiation. Further studies are required to clarify the precise lower limit of MF intensity and the MF intensity dependance.

The effects of static low MFs on the orientation and mechanical strength of newly formed bone or relationship between the two has not been reported. In a previous report in which a static high MF was applied for 60 h after rhBMP-2 pellet implantation, the effects on orientation were observed in osteoblasts (Kotani et al., 2002). In this study wherein a low MF was applied during the entire new bone formation process, the static low MF was found to change the orientation intensity of bone matrix and mechanical strength of rhBMP-2-induced newly formed bone in the direction perpendicular to the MF. Mature bone is formed through the deposition of collagen fibers secreted by osteoblasts, followed by the deposition of apatite crystals in the same direction as collagen fibers (Landis, 1995; Shin et al., 2017; Sasaki and Sudoh, 1997). In previous reports, with the application of static high MFs to adherent cells, such as osteoblasts in a collagen solution, cells were found to be aligned along collagen fibers, which were oriented perpendicular to the MF, because the generation of magnetic torque rotation is difficult in cells due to frictional and adhesive forces (Kotani et al., 2000; Eguchi et al., 2003). It is known that collagen fibers are oriented perpendicular to the high MF because the collagen molecule has a small negative diamagnetic susceptibility (O'Brien et al., 2016). It was reported that the apatite orientation, the mechanical properties of trabeculae, and the direction of the principal load stress are correlated with each other (Nakano et al., 2002; Ohman et al., 2007; Todoh et al., 2004). Our results suggest that static low MFs effect liberated collagen fibers during the process of bone formation and increase the orientation intensity of the bone matrix, which leads to an increase in mechanical strength, even with low MFs. However, there was no difference in the apatite orientation intensity in the major axis direction, which open windows exists though the direction is also perpendicular to the low MF. It is thought that the overlapping directions of angiogenesis and osteogenesis ensure that the effect of the MF is small in this direction.

The current study has few limitations. First, only 60 and 190 mT MF were used in this study. Permanent magnets with this MF strength are commercially available as health appliances and are easy to procure in our country. To optimize the effects of low MFs on bone formation, further experiments using magnets with different MF intensities need to be performed. Second, we chose compression tests to evaluate the mechanical strength of newly formed bone. Other mechanical tests including three-point bending tests and torsion tests are required to demonstrate the detailed mechanical properties. Third, we could not investigate the effects of low MF on endochondral bone formation and cortical bone. The investigations on the effects of low MF on a segmental long bone defect model are currently underway and we hope to clarify the effects of low MF on endochondral bone formation and cortical bone.

5. Conclusion

This study demonstrates that the application of low MFs promotes *in vitro* osteoblastic differentiation and *in vivo* ectopic bone formation. In addition, low MFs effected the orientation of cells *in vitro* and apatite crystals *in vivo*. As a result, mechanical strength in the direction perpendicular to the low MF increased. Thus, low MFs could be applied clinically to promote the early regeneration of bone with mechanical strength. In the future, verification with a bone defect model and with a bone close to the body surface will be necessary for clinical application.

Supplementary data to this article can be found online at https://doi.org/10.1016/j.bonr.2021.100757.

Transparency document

The Transparency document associated with this article can be found, in online version.

CRediT authorship contribution statement

T. Kaito, T. Nakano, and M. Kawakami were responsible for the study conception and design. R. Okada and T. Ishimoto collected the data, performed the analysis, and drafted the manuscript. R. Okada, J. Kodama, J. Kushioka, D. Tateiwa, Y. Ukon, and B. Zeynep contributed to animal surgery. K. Yamato created the apparatus. T. Kaito critically reviewed and contributed to the paper. All authors read and approved the final manuscript.

Declaration of competing interest

This study was funded by the Pip Corporation, Japan.

Acknowledgments

rhBMP-2 was kindly provided by Osteopharma Inc. This study was funded by the Pip Corporation, Japan.

References

Aydin, N., Bezer, M., 2011. The effect of an intramedullary implant with a static magnetic field on the healing of the osteotomised rabbit femur. Int. Orthop. 35 (1), 135–141.

G.K. Bruce, C.R. Howlett, R.L. Huckstep, Effect of a static magnetic field on fracture healing in a rabbit radius. Preliminary results, Clin Orthop Relat Res (222) (1987) 300–6.

Eguchi, Y., Ogiue-Ikeda, M., Ueno, S., 2003. Control of orientation of rat Schwann cells using an 8-T static magnetic field. Neurosci. Lett. 351 (2), 130–132.

T. Enomae, FiberOri8single03 V.8.03, 2019. http://www.enomae.com/FiberOri/FiberOri8s03.zip.

Enomae, T., Han, Y.-H., Isogai, A., 2006. Nondestructive determination of fiber orientation distribution of paper surface by image analysis. Nordic Pulp & Paper Research Journal 21 (2), 253–259.

Gao, J., Dennis, J.E., Muzic, R.F., Lundberg, M., Caplan, A.I., 2001. The dynamic in vivo distribution of bone marrow-derived mesenchymal stem cells after infusion. Cells Tissues Organs 169 (1), 12–20.

Higashi, T., Yamagishi, A., Takeuchi, T., Kawaguchi, N., Sagawa, S., Onishi, S., Date, M., 1993. Orientation of erythrocytes in a strong static magnetic field. Blood 82 (4), 1328–1334.

Ishimoto, T., Nakano, T., Umakoshi, Y., Yamamoto, M., Tabata, Y., 2013. Degree of biological apatite c-axis orientation rather than bone mineral density controls mechanical function in bone regenerated using recombinant bone morphogenetic protein-2. J. Bone Miner. Res. 28 (5), 1170–1179.

Ishimoto, T., Yamada, K., Takahashi, H., Takahata, M., Ito, M., Hanawa, T., Nakano, T., 2018. Trabecular health of vertebrae based on anisotropy in trabecular architecture and collagen/apatite micro-arrangement after implantation of intervertebral fusion cages in the sheep spine. Bone 108, 25–33.

Kanda, Y., 2013. Investigation of the freely available easy-to-use software 'EZR' for medical statistics. Bone Marrow Transplant. 48 (3), 452–458.
Kim, E.C., Park, J., Kwon, I.K., Lee, S.W., Park, S.J., Ahn, S.J., 2017. Static magnetic fields promote osteoblastic/cementoblastic differentiation in osteoblasts, cementoblasts, and periodontal ligament cells. J Periodontal Implant Sci 47 (5), 273–291.
Kotani, H., Iwasaka, M., Ueno, S., Curtis, A., 2000. Magnetic orientation of collagen and bone mixture. J. Appl. Phys. 87 (9), 6191–6193.
Kotani, H., Kawaguchi, H., Shimoaka, T., Iwasaka, M., Ueno, S., Ozawa, H., Nakamura, K., Hoshi, K., 2002. Strong static magnetic field stimulates bone formation to a definite orientation in vitro and in vivo. J. Bone Miner. Res. 17 (10), 1814–1821.
Landis, W.J., 1995. The strength of a calcified tissue depends in part on the molecular structure and organization of its constituent mineral crystals in their organic matrix. Bone 16 (5), 533–544.
Matsugaki, A., Aramoto, G., Ninomiya, T., Sawada, H., Hata, S., Nakano, T., 2015. Abnormal arrangement of a collagen/apatite extracellular matrix orthogonal to osteoblast alignment is constructed by a nanoscale periodic surface structure. Biomaterials 37, 134–143.
Murray, H.B., Pethica, B.A., 2016. A follow-up study of the in-practice results of pulsed electromagnetic field therapy in the management of nonunion fractures. Orthop. Res. Rev. 8, 67–72.
Nakano, T., Kaibara, K., Tabata, Y., Nagata, N., Enomoto, S., Marukawa, E., Umakoshi, Y., 2002. Unique alignment and texture of biological apatite crystallites in typical calcified tissues analyzed by microbeam X-ray diffractometer system. Bone 31 (4), 479–487.
O'Brien, W., Fissel, B.M., Maeda, Y., Yan, J., Ge, X., Gravallese, E.M., Aliprantis, A.O., Charles, J.F., 2016. RANK-independent osteoclast formation and bone erosion in inflammatory arthritis. Arthritis Rheumatol 68 (12), 2889–2900.
Ohman, C., Baleani, M., Perilli, E., Dall'Ara, E., Tassani, S., Baruffaldi, F., Viceconti, M., 2007. Mechanical testing of cancellous bone from the femoral head: experimental errors due to off-axis measurements. J. Biomech. 40 (11), 2426–2433.
Sadri, M., Abdolmaleki, P., Abrun, S., Beiki, B., Samani, F.S., 2017. Static magnetic field effect on cell alignment. Growth, and Differentiation in Human Cord-Derived Mesenchymal Stem Cells, Cell Mol Bioeng 10 (3), 249–262.
Sasaki, N., Sudoh, Y., 1997. X-ray pole figure analysis of apatite crystals and collagen molecules in bone. Calcif. Tissue Int. 60 (4), 361–367.
Schenck, J.F., 2000. Safety of strong, static magnetic fields. J. Magn. Reson. Imaging 12 (1), 2–19.
Shin, K., Acri, T., Geary, S., Salem, A.K., 2017. Biomimetic mineralization of biomaterials using simulated body fluids for bone tissue engineering and regenerative medicine. Tissue Eng Part A 23 (19–20), 1169–1180.
Shinohara, H., Takei, H., Saito, D., Kotani, M., Ueno, S., Nakahira, A., 2006. Fundamental study on bone formation using collagen orientation induced by magnetic fields. J. Ceram. Soc. Jpn. 114 (1325), 131–134.
Teodori, L., Albertini, M.C., Uguccioni, F., Falcieri, E., Rocchi, M.B., Battistelli, M., Coluzza, C., Piantanida, G., Bergamaschi, A., Magrini, A., Mucciato, R., Accorsi, A., 2006. Static magnetic fields affect cell size, shape, orientation, and membrane surface of human glioblastoma cells, as demonstrated by electron, optic, and atomic force microscopy. Cytometry A 69 (2), 75–85.
Todoh, M., Ihara, M., Matsumoto, T., Tanaka, M., 2004. Relationship between mechanical property of cancellous bone and hardness of trabeculae. JSME International Journal Series C 47 (4), 1075–1078.
Umeno, A., Ueno, S., 2003. Quantitative analysis of adherent cell orientation influenced by strong magnetic fields. IEEE Trans Nanobioscience 2 (1), 26–28.
Yamamoto, Y., Ohsaki, Y., Goto, T., Nakasima, A., Iijima, T., 2003. Effects of static magnetic fields on bone formation in rat osteoblast cultures. J. Dent. Res. 82 (12), 962–966.
Yuge, L., Okubo, A., Miyashita, T., Kumagai, T., Nikawa, T., Takeda, S., Kanno, M., Urabe, Y., Sugiyama, M., Kataoka, K., 2003. Physical stress by magnetic force accelerates differentiation of human osteoblasts. Biochem. Biophys. Res. Commun. 311 (1), 32–38.
Yun, H.M., Ahn, S.J., Park, K.R., Kim, M.J., Kim, J.J., Jin, G.Z., Kim, H.W., Kim, E.C., 2016. Magnetic nanocomposite scaffolds combined with static magnetic field in the stimulation of osteoblastic differentiation and bone formation. Biomaterials 85, 88–98.